JOURNAL OF MATERIALS SCIENCE 18 (1983) 525–532

Characterization of AlN ceramics containing long-period polytypes

G. VAN TENDELOO*, K. T. FABER, G. THOMAS
Department of Materials Science and Mineral Engineering, University of California, Berkeley, California 94720, USA

Two AlN–SiO_2 materials have been investigated by means of electron microscopy; fracture toughness has been used to characterize both materials. Three new long-period polytypes, close to the 2H hexagonal AlN structure, have been identified by high-resolution electron microscopy, namely 33R, 24H and 39R. These polytypes are built on the same stacking principle as those in the previously observed shorter polytypes in the AlN system. Indentation measurements indicate similar hardness and toughness for the different polytypes in these ceramics.

1. Introduction

Since the discovery 10 years ago of the β'-phase in the Si–Al–O–N system [1–3], the Si_3N_4–AlN–Al_2O_3–SiO_2 quasi-equilibrium phase diagram has been widely studied (see e.g. [4]), mainly because of its possible high-temperature applications in ceramics technology.

The AlN-polytype group, situated in the phase diagram between β'-sialon and AlN [4, 5] has been identified as $Al_{x+y}Si_{6-x}O_xN_{8-x+y}$. Each phase extends along a line of constant metal to non-metal ratio and has a narrow range of homogeneity. Such series are not unusual and have been reported in Be–Si–O–N [6, 7], Mg–Si–Al–O–N and Li–Si–Al–O–N (see e.g. [4]).

The structure of the AlN-prototypes is based on the 2H-AlN structure (wurtzite type) with approximate unit cell dimensions [4], $a = 0.311$ nm, and $c = 0.499$ nm. Fig. 1 represents this basic structure together with its projections along [00.1] and [10.0]. The metal atoms (Al) form an hexagonal close-packed arrangement and the non-metal atoms (N) fill one-half of the available tetrahedral sites (e.g. all tetrahedra pointing down (indicated by 1 in Fig. 1c) giving rise to the composition Al_1N_1. When the metal to non-metal ratio (M/X) decreases (reaching a minimum at 1/2 when all tetrahedra are occupied), the non-metal ions have to fill adjacent tetrahedra which share common faces (1 and 2 in Fig. 1c). This would give rise to impossibly short interatomic distances between non-metal atoms which can only be avoided if the metal atom configuration is locally changed from hexagonal (ABAB ...), to cubic (ABC ...), i.e. by introducing a stacking fault in the metal ion configuration. Such a stacking fault configuration projected along [10.0] is depicted in Fig. 2; filled tetrahedra are shaded. An excess of non-metal atoms can be taken up in the faulted region (indicated between the arrows in Fig. 2) where the tetrahedra share only an edge, increase significantly the interatomic non-metal distance. It is known that for the AlN-rich compositions of the sialon system, the excess non-metal atoms are taken up by creating periodic stacking faults in the metal configuration and filling up a double layer of tetrahedra at every fault [4]. It is clear that the further the M/X ratio deviates from 1, the closer is the stacking-fault spacing. They are never observed closer than every 4th layer or further separated than every 9th layer; the identified polytypes (using the Ramsdell notation [8]) are 8H, 15R, 12H, 21R and 27R [4]. When $9/10 < M/X < 1$, it is assumed that the extra non-metal atoms are taken up in the 2H phase forming the so-called $2H^{\delta}$ structure; it is essentially the 2H structure but with an elongated c-parameter (e.g. [4]).

*Permanent address: RUCA, University of Antwerp, Groenenborgerlaan 171, B2020, Belgium.

0022–2461/83/020525–08$03.46/0

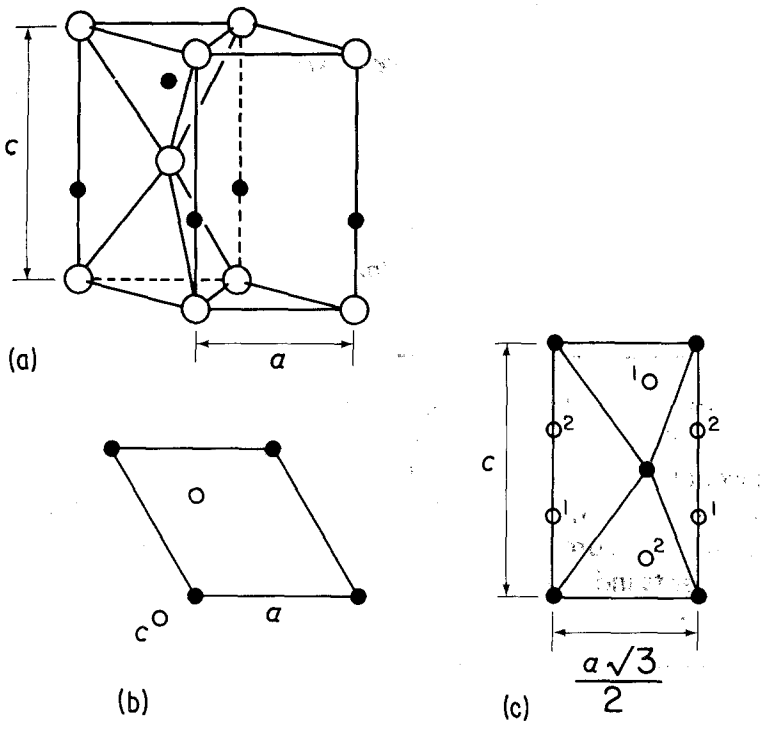

Figure 1 (a) Spatial view of the basic 2H wurtzite structure. Metal atoms are represented by large open circles; anions are represented as small closed circles. (b) Projection of the 2H-structure along [00.1]; the non-metal atoms project along the metal atom configuration. (c) Projection of 2H along [10.0]. The centres of two different tetrahedra are indicated as 1 and 2.

In the Si_3N_4 end of the phase diagram, small variations in composition can alter the amount and viscosity of the grain-boundary glassy phase which, in turn, modifies the grain structure and mechanical behaviour at both elevated temperatures and at room temperature [9–12]. However, the relationship between slight variations in composition (and consequently in polytype) and mechanical behaviour has not been explored in detail in the $Al_{x+y}Si_{6-x}O_xN_{8-x+y}$ corner of the diagram, although preliminary studies by Komeya and Tsuge [13] indicated that the fracture strengths depend on processing conditions (as listed in Table I).

It is our intent here to characterize two materials in the AlN–SiO_2 system with similar net compositions but differing in processing conditions. Of prime interest is the polytype characterization of the two materials. In addition, the fracture toughness of the two materials is examined in the light of the fracture strength differences.

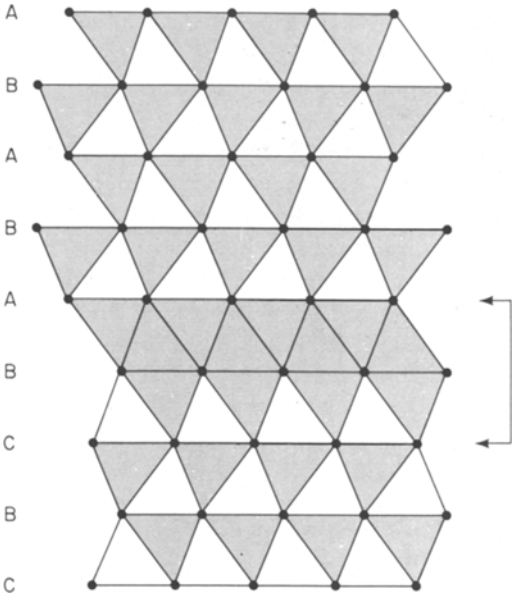

Figure 2 [10.0] projection of a stacking fault in the basic 2H-structure locally creating an ABC cubic stacking. Shaded tetrahedra are those to be filled by anions.

2. Experimental procedure

Specimens for electron microscopy and fracture toughness measurements were kindly provided

TABLE I Mechanical strength of two AlN–SiO_2 ceramics (from Komeya and Tsuge [13])

Temperature (° C)	Flexural strength (MPa)	
	A'*	B'*
R.T.	460	265
1200	440	330
1600	370	215
1700	380	225

*See Section 2.

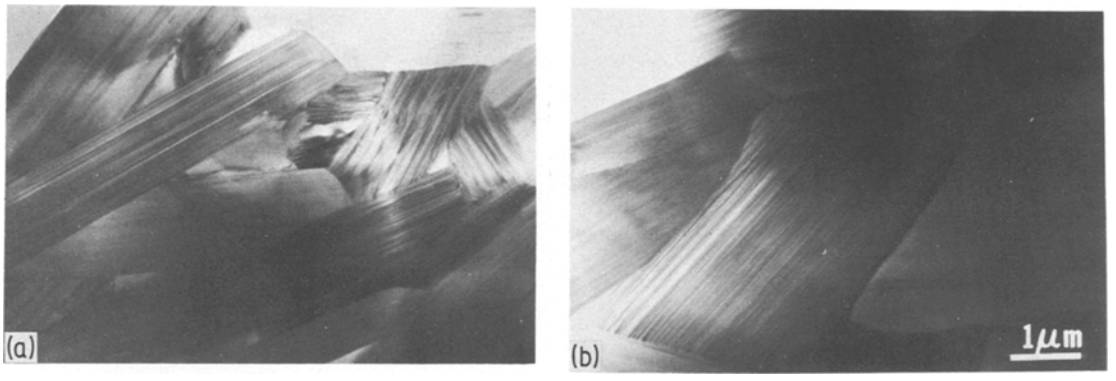

Figure 3 Low-magnification micrographs of (a) A′ and (b) B′ specimens.

by Dr K. Komeya (Toshiba Corp., Japan). They were prepared by hot-pressing 90 wt% AlN and 10 wt% SiO_2 at 2100° C at a stress of 500 kg cm^{-2} for 120 min (sample A′) or 300 min (sample B′) after pre-reaction in N_2 at 2000° C [13]. Samples used for the present investigation refer to materials designated A′ and B′ by Komeya and Tsuge [13].

For electron microscopy investigation, the bars were sliced along the pressing direction to obtain 2.3 mm diameter discs for thinning by ion milling. Final specimens were carbon-coated to improve the electrical conductivity and were examined in a Jeol 200CX electron microscope. Laser optical diffraction was used to obtain microdiffraction patterns.

The fracture toughness of the two materials was measured using the indentation method designed by Evans and Charles [14]. Indentations were made using a Vickers pyramid indentor, loaded with 10 to 20 N, on to optically polished surfaces. From the post-indentation analysis, the fracture toughness, K_c, can be calculated using the expression [15]:

$$K_c = 0.016 (E/H)^{1/2} (P/c_0^{3/2}) \quad (1)$$

where E is the elastic modulus, H, the hardness ($= 0.47 P/a^2$), P the peak load, c_0 the radial crack length (emanating from the indentation) and $2a$, the indentation length. Thus, the indentation method provides not only a measure of the hardness but also of the fracture toughness.

3. Observations

3.1. Electron microscopy

Specimens A′ and B′, hot-pressed for different periods, were reported to have different grain sizes from scanning electron microscopy, but according to X-ray diffraction, both were proposed to have the same 27R polytypes structure [13].

Low-magnification transmission electron microscopy reveals this difference in morphology (Fig. 3). A′ grains are small, with a thickness in the c-direction of 1 to 2 μm. The long laths show a close resemblance to the morphology of α-SiC in a β-SiC matrix [16]. In the B′ material the laths are at least twice as thick and less elongated than in the A′ material.

3.2. Electron diffraction

Selected-area electron diffraction from the individual grains confirms the existence of polytypes based on the 2H structure but, instead of the 27R polytype suggested by Komeya and Tsuge from X-ray measurements [13], longer period polytypes were detected. Moreover, the kind of polytypes was dependent upon the length of hot-pressing (i.e. specimen A′ or B′). A series of [10.0] diffraction patterns identifying the polytypes 27R, 33R, 24H and 39R, together with the basic 2H structure is shown in Fig. 4. The basic reflections corresponding to the interplanar close-packed spacing are indicated by arrows. The B′ material mainly consisted of 27R with some laths of the 33R structure while the A′ material consisted mainly of 33R, 24H and 39R with some areas of 2H. The 27R polytype was never found in these latter specimens. Most of the diffraction patterns showed irregular mixtures of different polytypes producing streaked diffraction patterns in the central as well as in the non-central rows. Other patterns have sharp, well-defined reflections in the central rows, but show streaking or spot-doubling in the off-central rows; this is striking, e.g. in Fig. 4b, and can be attributed to twinning

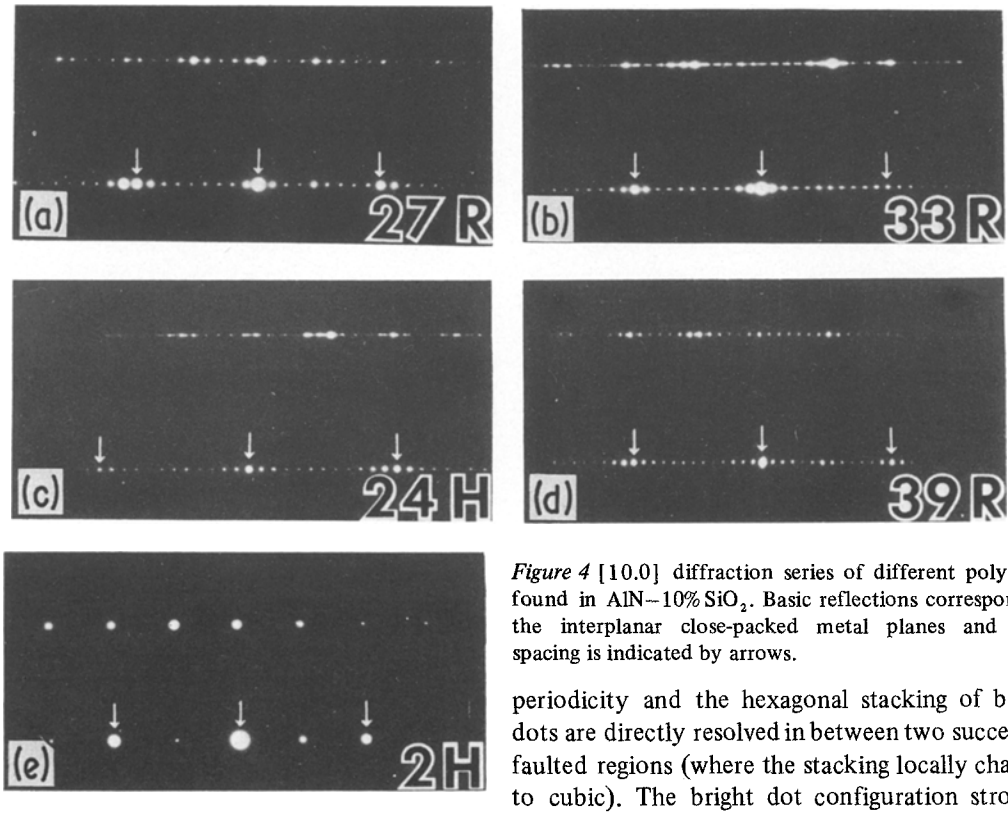

Figure 4 [10.0] diffraction series of different polytypes found in AlN–10% SiO_2. Basic reflections correspond to the interplanar close-packed metal planes and their spacing is indicated by arrows.

on the close-packed planes. In all rhombohedral structures this plane is not a mirror plane, and twinning is frequently observed in rhombohedral polytypes [7, 17].

3.3. High-resolution electron microscopy

While electron diffraction will provide information concerning the overall or average stacking sequence, high-resolution electron microscopy imaging is particularly suitable for studying local deviations from the ideal stacking sequence (e.g. [7, 17]) or to analyse defects on an atomic scale, e.g. [18].

All of the high-resolution observations reproduced here were taken with the electron beam along [10.0] when referring to the 2H wurtzite basic structure. A [10.0] diffraction pattern also indicating the size of the objective aperture used for all direct imaging is reproduced in Fig. 5. The instrument used for imaging has a Scherzer resolution limit (or a first cut-off in the transfer function) of 0.25 nm, enabling one to resolve the close-packed interplanar spacing and to obtain atomic scale information about the stacking sequence of subsequent layers.

An image of a perfect 33R polytype region (Fig. 4b) is produced in Fig. 6. The 11-layer periodicity and the hexagonal stacking of bright dots are directly resolved in between two successive faulted regions (where the stacking locally changes to cubic). The bright dot configuration strongly resembles the metal atom configuration when projected along [10.0] (see Fig. 2). This is even more striking from Fig. 7b which shows in detail the interface between the basic 2H region (right) and the polytype region (left). However, until calculations have been performed to simulate the images as a function of thickness and focus,

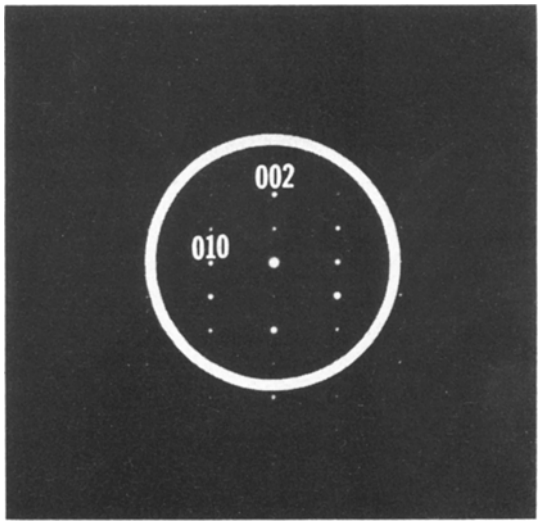

Figure 5 [10.0] electron diffraction pattern of 2H AlN; the size of the objective aperture has been indicated.

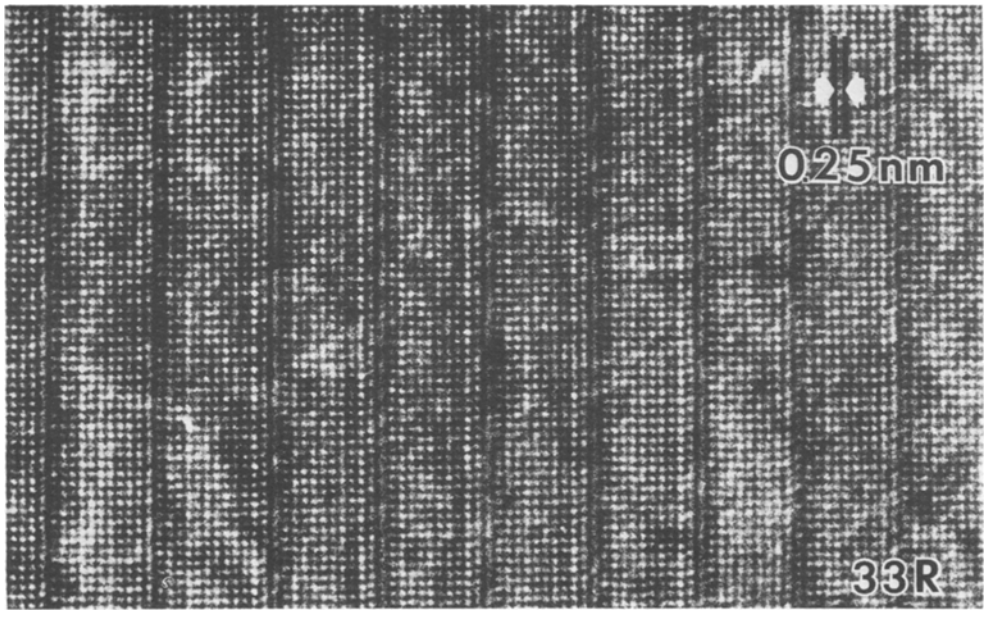

Figure 6 High-resolution electron micrograph of a 33R polytype in AlN–SiO_2.

it is not possible to correlate the bright dots with the Al cation positions; all that can be said now is that the bright dot *configuration* is closely related to the metal atom configuration. It is certainly impossible without calculations (and probably also with the calculated images) to obtain information about the non-metal configuration in the boundary region between two hexagonal bands (e.g. to decide whether all tetrahedra within this area are filled (see Fig. 2).

Fig. 7 is interesting in different respects: it shows that within one grain the parent 2H structure can coexist with the polytype structure. Such behaviour has only been found for long-period polytypes (24H or 39R); suggesting that longer polytypes are unlikely and that the structure will transform to what has been termed the $2H^{\delta}$ structure. Fig. 7a, at lower magnification, illustrates the heavy faulting in the polytype structure; the bands U and V are twin-related, which can be deduced from their contrast differences as has been shown in previous studies of other systems, e.g. in $BeSiN_2$ [7] or in Ba-ferrites [19]. The high-resolution image of Fig. 7b reveals a stacking fault (the boundary between the 2H and the 24H polytype) which stops in the matrix terminating at a dislocation. When viewed along the close-packed planes, it is clear that a plane has been removed from the 2H configuration in order to create the fault and hence the polytype.

Very often adjacent grains develop, having a common *a*-axis, and in a number of cases the basal (*a-b*) plane is parallel to one of the prismatic planes. Such behaviour is observed in Fig. 8, and the diffraction pattern showing the exact orientation relationship between two 39R polytypes is reproduced in the inset. Such intergrowth is stimulated because the (00.2) spacing is almost identical to the (01.0) spacing. The interface, however, is not strictly planar.

3.4. Fracture toughness measurements

Indentation measurements (based on an estimated elastic modulus of 285 GPa) indicated essentially similar hardness and toughness levels for both materials ($H \simeq 14.7$ GPa, $K_c \simeq 2.4$ MPa $m^{1/2}$). These mechanical properties are similar to those encountered in sintered α-SiC.

One noticeable feature of the indentations was the poor quality of the indentations at higher loads. Measurements using loads greater than 20 N were not possible, as chipping resulted around the indentation. This behaviour is not uncommon in materials with a high hardness-to-fracture toughness ratio (H/K_c), e.g. sapphire, SiC and B_4C [20].

4. Discussion

The present observations clearly show that three new long-period polytypes have been identified in the AlN-polytype series of the sialon quasi-

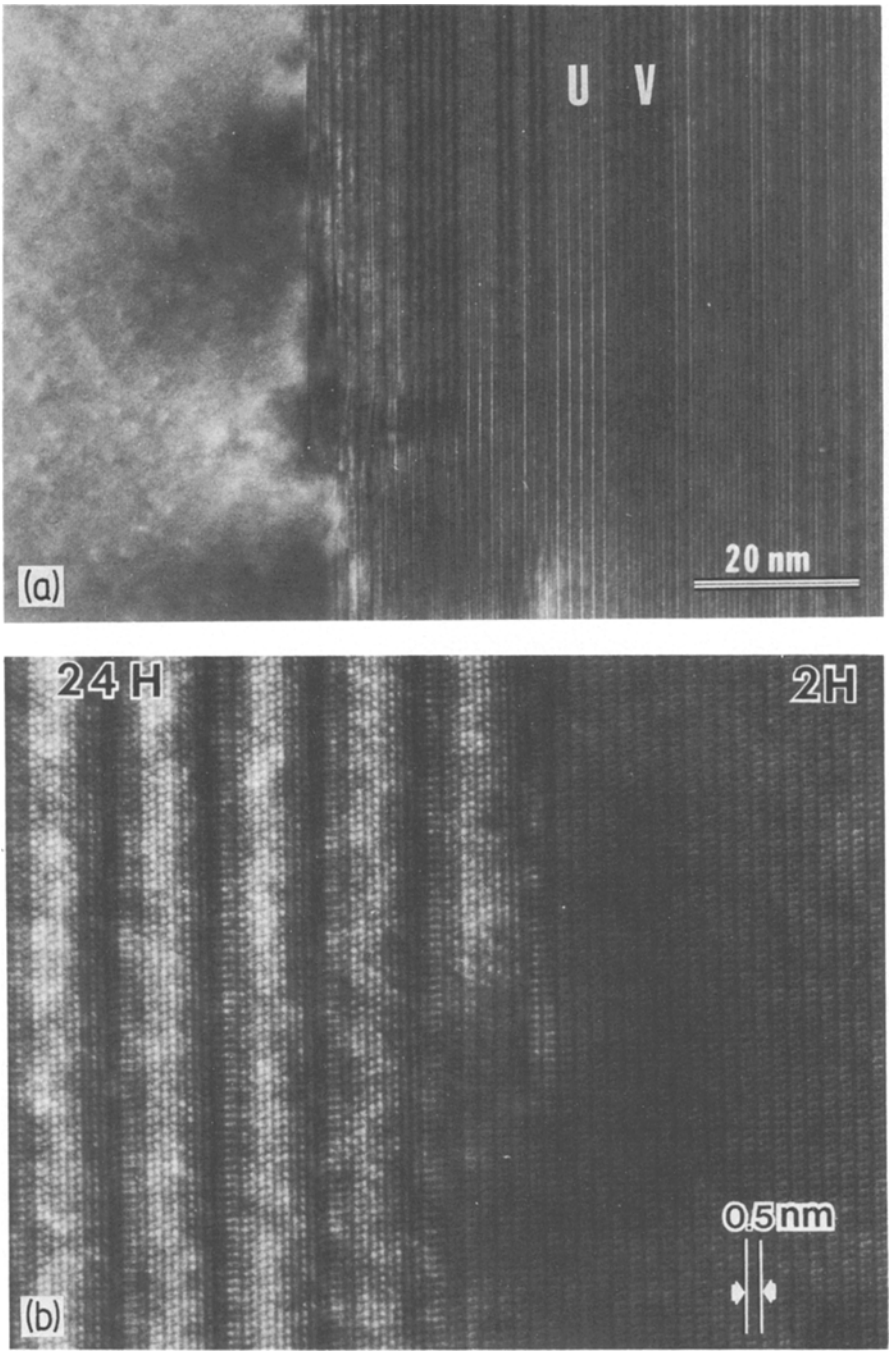

Figure 7 (a) Relatively low magnification of the interface between 2H and an irregular polytype region. (b) High-resolution micrograph of a similar region to (a).

equilibrium phase diagram; namely, 33R, 24H and 39R. Assuming that the same structure as the previously determined polytypes (8H, 15R, 12H, 21R and 27R) is maintained (i.e. the excess non-metal atoms are stacked along the stacking faults), the new polytypes correspond to M/X ratios 11/12, 12/13 and 13/14. Different polytypes in materials A′ and B′ therefore suggest small differences in composition must occur as a result of their slightly differing preparation.

Table II provides a summary of the now identified AlN-polytypes where n is the number of metal

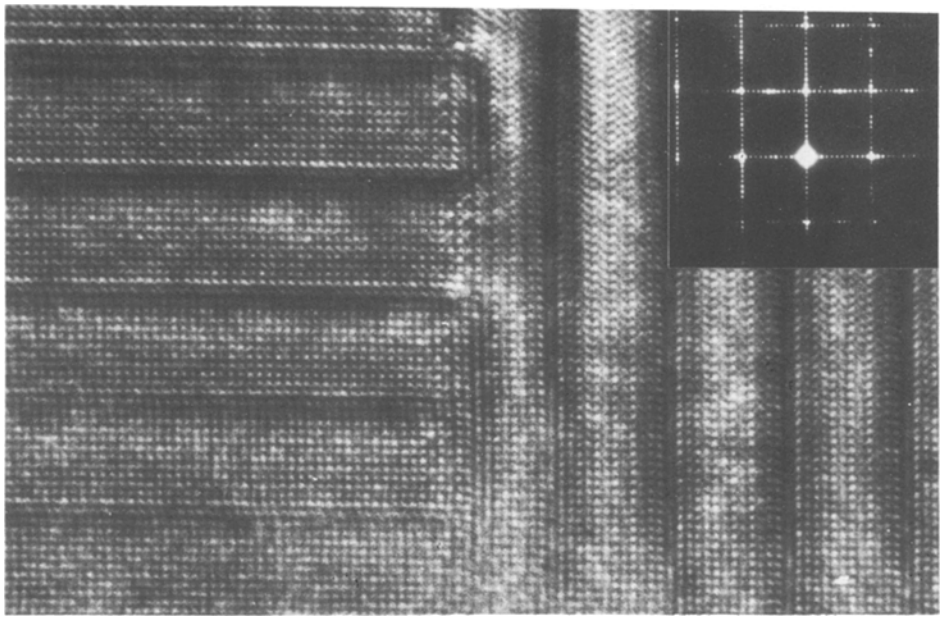

Figure 8 High-resolution image of a grain boundary between two polytype grains having exactly perpendicular *c*-axes but a common *a*-axis (parallel to the beam).

planes between subsequent stacking faults. The relative interplanar close-packed spacing for the long-period polytypes with respect to the 2H-structure is easily measured from the diffraction patterns taken over areas containing both 2H and the polytype. In Fig. 9 the reflection belonging to 2H are marked by arrows. The measured interplanar spacings perfectly fit the linear relationship between the interplanar spacing the MX_2 layer concentration measured by Jack [4].

Despite the differences in polytypes comprising the two materials examined, no significant difference in fracture toughness was observed. Furthermore, differences in fracture toughness cannot be used to explain the variations in flexural strengths measured by Komeya and Tsuge [13]. More likely, strength variations are due to the grain, and/or pore size differences in the two materials, where the average grain or pore size is equivalent to the size of the critical flaw, as has been observed in numerous large-grained ceramic materials.

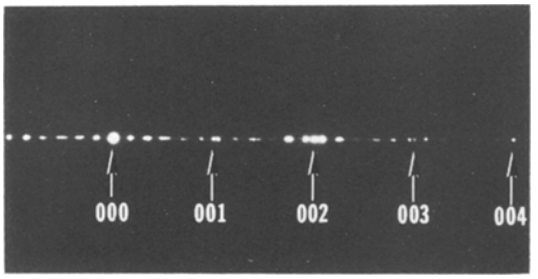

Figure 9 [10.0] diffraction pattern taken across the interface between the basic 2H structure and a long-period polytype structure.

Acknowledgements

This work was supported by NSF Grant DMR 802 3461. Support for KTF was provided by the Carborundum Company, Niagara Falls, New York. The authors are grateful to L. Andersen for the preparation of electron microscopy samples and to A. G. Evans for helpful discussions.

References

1. K. H. JACK and W. I. WILSON, *Nature Phys. Sci.* **23E** (1972) 28.

TABLE II

n	M/X	Polytype	Interplanar $d_{00.2}$ spacing	Reference
4	4/5	8H	2.88	[4]
5	5/6	15R	2.79	[4]
6	6/7	12H	2.74	[4]
7	7/8	21R	2.72	[4]
9	9/10	27R	2.67	[4]
11	11/12	33R	2.62	Present work
12	12/13	24R	Not measured	Present work
13	13/14	39R	2.60	Present work
∞	1	2H	2.49	[4]

2. Y. OYAMA and O. KAMIGAITO, *Jap. J. Appl. Phys.* **10** (1972) 1637.
3. K. H. JACK, "Phase diagrams: Materials Science and Technology" Vol. 6-V of "Refractory Materials", edited by A. M. Alpen (Academic Press, New York, 1978) p. 241.
4. K. H. JACK, *J. Mater. Sci.* **11** (1976) 1135.
5. L. J. GLAUCKLER, H. L. LUKAS and G. PETZOW, *J. Amer. Ceram. Soc.* **58** (1975) 346.
6. D. P. THOMPSON, *J. Mater. Sci.* **11** (1976) 1377.
7. T. M. SHAW and G. THOMAS, *J. Solid State Chem.* **33** (1980) 63.
8. L. S. RAMSDELL, *Amer. Mineral.* **32** (1947) 64.
9. F. L. RILEY (ed.), "Nitrogen Ceramics" (Nordhoff Press, Leydan, 1976).
10. A. TSUGE, K. NISHIDA and M. KOMATSU, *J. Amer. Ceram. Soc.* **58** (1975) 323.
11. D. R. CLARKE, "Nitrogen Ceramics", edited by F. L. Riley (Nordhoff Press, Leydan, 1976) p. 433.
12. F. F. LANGE, *Int. Metals Rev.* **247** (1980) 1.
13. K. KOMEYA and A. TSUGE, *Yogyo-Kyokai-Shi* **89** (1981) 615.
14. A. G. EVANS and E. A. CHARLES, *J. Amer. Ceram. Soc.* **59** (1976) 371.
15. B. R. LAWN, A. G. EVANS and D. B. MARSHALL, *J. Amer. Ceram. Soc.* **63** (1980) 574.
16. A. H. HEUER, G. A. FRYBERG, L. OGBUGI, T. E. MITCHELL and S. SHINOSAKI, *ibid.* **61** (1978) 406.
17. J. VAN LANDUYT, G. VAN TENDELOO and S. AMELINCKX, to be published (1982).
18. J. H. SPENCE, "Experimental High Resolution Electron Microscopy" (Clarendon Press, Oxford, 1981).
19. J. VAN LANDUYT, S. AMELINCKX, J. A. KOHN and D. W. ECKART, *J. Solid State Chem.* **9** (1974) 103.
20. T. UCHIYAMA, D. B. MARSHALL and A. G. EVANS, *J. Amer. Ceram. Soc.* (1983) to be published.

Received 1 June
and accepted 14 July 1982